Pergamon

PII: S0191–8141(98)00116–8

Journal of Structural Geology, Vol. 20, No. 5, pp. 655 to 660, 1998

0191-8141/98 $19.00 + 0.00

Brevia

SHORT NOTE

Brittle failure mode plots for compressional and extensional tectonic regimes

RICHARD H. SIBSON

Department of Geology, University of Otago, P.O. Box 56, Dunedin, New Zealand

(*Received* 5 *August* 1997; *accepted in revised form* 8 *December* 1997)

Abstract—Equations governing different macroscopic modes of brittle rock failure (extensional fracturing, extensional-shear fracturing, compressional shear failure and reshear of existing faults) can be represented on plots of differential stress vs effective vertical stress for a set of material properties. Such plots can be constructed for different tectonic regimes and correlated to depth for particular fluid pressure conditions, allowing easy evaluation of the physical controls on brittle rock failure, and ready comparison of the fields occupied by the three failure modes in different tectonic settings. They emphasize the relative ease, in terms of differential stress and fluid-pressure levels, of deforming a rock mass by brittle fracturing and faulting in extensional regimes compared with compressional. Aside from their relevance to general structural mechanics, these generic failure plots have wide-ranging application to understanding the initial development and progressive evolution of fault–fracture systems, both in sedimentary basins and as hosting structures for hydrothermal mineralization in different tectonic settings.

INTRODUCTION

The representation of 2-D stress states in relation to a brittle failure envelope on a Mohr diagram (Fig. 1) has proved immensely useful in the evaluation of rock mass stability and the stress conditions under which different modes of brittle failure may occur (e.g. Jaeger and Cook, 1979). However, one shortcoming of this technique is the difficulty of transcribing the physical conditions for various modes of brittle failure to particular depth and fluid-pressure regimes in the crust. This note outlines a simple method for constructing brittle failure maps defining the stress and fluid-pressure conditions for different modes of brittle failure at varying depths in compressional and extensional tectonic settings.

MACROSCOPIC FAILURE CRITERIA

In fluid-saturated crust under triaxial stress, the effective principal compressive stresses are:

$$\sigma'_1 = (\sigma_1 - P_f) > \sigma'_2 = (\sigma_2 - P_f) > \sigma'_3 = (\sigma_3 - P_f) \quad (1)$$

where P_f is the fluid pressure (Hubbert and Rubey, 1959). At a depth, z, in crust with average density, ρ, the level of fluid pressure may be related to the vertical stress, σ_v, by means of the pore-fluid factor:

$$\lambda_v = \frac{P_f}{\sigma_v} = \frac{P_f}{\rho g z} \quad (2)$$

where g is gravitational acceleration. The effective vertical stress is then:

$$\sigma'_v = (\sigma_v - P_f) = \rho g z(1 - \lambda_v). \quad (3)$$

For a compressional tectonic regime in the upper crust, $\sigma_v = \sigma_3$, while for an extensional regime, $\sigma_v = \sigma_1$ (Anderson, 1951).

A composite failure envelope for intact isotropic rock (Fig. 1) normalized to tensile strength, T (assumed finite), may be constructed by merging the macroscopic Griffith criterion with the Coulomb criterion for compressional shear failure on a Mohr diagram with shear stress, τ, plotted against effective normal stress, $\sigma_n' = (\sigma_n - P_f)$ (Brace, 1960; Secor, 1965). The macroscopic Griffith criterion (Griffith, 1924) is of parabolic form:

$$\tau^2 = 4\sigma'_n T + 4T^2 \quad (4)$$

and predicts a shear strength, $\tau = 2T$ when $\sigma'_n = 0$. The linear Coulomb criterion may be written:

$$\tau = C + \mu_i \sigma'_n = C + \mu_i(\sigma_n - P_f) \quad (5)$$

for a rock mass with cohesive shear strength, C, and coefficient of internal friction, μ_i. From a compilation of laboratory strength tests on different rock types, Jaeger and Cook (1979, p. 155) found coefficients of internal friction lying generally within the range, $0.5 < \mu_i < 1.0$. They also noted that the expected relationship $C \approx 2T$ holds only very approximately.

A 'generic' failure envelope normalized to the tensile strength, T, has been constructed here (Fig. 1) by adopting an average value for internal friction,

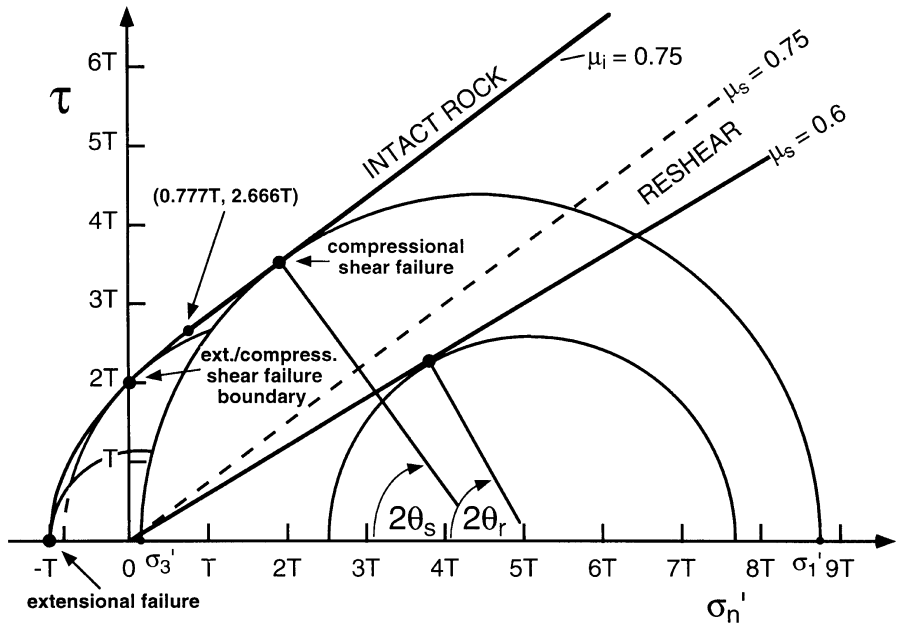

Fig. 1. Generic Mohr diagram showing a composite Griffith–Coulomb failure envelope for intact rock normalized to tensile strength, T, with $\mu_i = 0.75$ in the compressional field, plus reshear criteria for cohesionless faults with $\mu_s = 0.6$ and 0.75. Critical stress circles are shown representing different failure modes for intact rock and a reshear stress state for an optimally oriented existing fault with $\mu_s = 0.6$. μ_i is internal friction of intact rock; μ_s is static friction for reshear.

$\mu_i = 0.75$, for the Coulomb criterion which merges with the Griffith criterion in (σ_n', τ) space at the point (0.777 T, 2.666 T). This corresponds to a Coulomb criterion with $C = 2.083\,T$. For a composite failure envelope of this kind, three different modes of brittle failure of intact rock may be recognized.

Extensional fracturing

Pure extension fractures form perpendicular to σ_3 for critical stress states represented by circles touching the failure envelope uniquely at the point ($-T$, 0) such that:

$$\sigma_3' = -T \quad \text{or} \quad P_f = \sigma_3 + T. \tag{6}$$

This can only occur when the differential stress (corresponding to the diameter of the stress circle) satisfies the condition, $(\sigma_1 - \sigma_3) < 4T$. For compressional tectonic regimes ($\sigma_v = \sigma_3$), this criterion becomes:

$$\sigma_v' = -T \tag{7}$$

while for extensional regimes ($\sigma_v = \sigma_1$) it may be written:

$$(\sigma_1 - \sigma_3) = \sigma_v' + T. \tag{8}$$

Extensional-shear fractures

Hybrid extensional-shear fractures (Hancock, 1985) form when a critical stress circle with a diameter in the range, $4\,T < (\sigma_1 - \sigma_3) < 5.66\,T$, touches the parabolic part of the failure envelope in the tensile field ($\sigma_n' < 0$). At failure, a combination of shear and extensional opening occurs across a fracture which contains the σ_2 direction and lies at an angle, θ_{es}, to the σ_1 direction with $0 < \theta_{es} < \theta_s$ (see below). The macroscopic Griffith criterion (equation 4) may be expressed in terms of the principal stresses at failure as:

$$(\sigma_1 - \sigma_3)^2 = 8T(\sigma_1' + \sigma_3') \tag{9}$$

(Jaeger and Cook, 1979). For a compressional tectonic regime, this expression reduces to:

$$(\sigma_1 - \sigma_3) = 4T \pm 4\sqrt{(T^2 + T\sigma_v')} \tag{10}$$

while for an extensional regime it becomes:

$$(\sigma_1 - \sigma_3) = -4T \pm 4\sqrt{(T^2 + T\sigma_v')} \tag{11}$$

Compressional shear failure (faulting)

Faults (shear fractures) form by compressional shear failure when a stress circle with $(\sigma_1 - \sigma_3) > 5.66\,T$ touches the failure envelope in the compressional field ($\sigma_n' > 0$). For the linear (Coulomb) portion of the failure envelope, such faults form along planes containing the σ_2 direction and lying at an angle, $\theta_s = 0.5\,\tan^{-1}(1/\mu_i)$ to the σ_1 direction. For $\mu_i = 0.75$, $\theta_s \approx 27^\circ$. The Coulomb criterion (equation 5) may be rewritten in terms of the principal stresses at failure as:

$$(\sigma_1 - \sigma_3) = 2C\sqrt{K} + (K - 1)\sigma_3' \tag{12}$$

where $K = [\sqrt{(1 + \mu_i^2)} + \mu_i]^2$ (Jaeger and Cook, 1979). For the composite envelope, $K = 4$ when $\mu_i = 0.75$, and $C = 2.083\,T$. For a tectonic regime involving hori-

zontal compression the expression reduces to:

$$(\sigma_1 - \sigma_3) = 8.33\ T + 3\sigma'_v; \quad (13)$$

while for an extensional regime it becomes:

$$(\sigma_1 - \sigma_3) = 2.083\ T + 0.75\sigma'_v \quad (14)$$

Reshear of a cohesionless fault

The reactivation criterion for reshear of an existing cohesionless fault is:

$$\tau = \mu_s \sigma'_n = \mu_s(\sigma_n - P_f) \quad (15)$$

where μ_s is the static coefficient of rock friction, and is also shown in Fig. 1. For existing faults whose poles lie in the plane containing σ_1 and σ_3, this expression may be rewritten in terms of the effective principal stresses as

$$\frac{\sigma'_1}{\sigma'_3} = \frac{(\sigma_1 - P_f)}{(\sigma_3 - P_f)} = \frac{(1 + \mu_s \cot\theta_r)}{(1 - \mu_s \tan\theta_r)} \quad (16)$$

where θ_r is the reactivation angle between σ_1 and the plane (Sibson, 1985). The optimal reactivation angle, for which the stress ratio reaches a positive minimum, occurs when $\theta_r = 0.5\ \tan^{-1} 1/\mu_s$. From an extensive series of laboratory sliding experiments on rock friction, Byerlee (1978) found μ_s to be largely independent of rock type and confined within the range, $0.6 < \mu_s < 0.85$.

For a 'mature' fault with a well established gouge zone, Lockner and Byerlee (1993) determined a simple relationship,

$$\mu_{as} = \sin(\tan^{-1} \mu_i) \quad (17)$$

between the internal friction, μ_i, of a particular rock type and the apparent friction, μ_{as}, of a gouge layer derived from that rock. For the 'generic' value of internal friction ($\mu_i = 0.75$) adopted here, $\mu_s = \mu_{as} = 0.6$, at the bottom of the Byerlee range. However, because we are not solely concerned with mature fault zones, a representative value near the middle of the Byerlee range ($\mu_s = 0.75$), with the same slope as the intact rock criterion, is also plotted as an alternative reshear criterion (Fig. 1). For $\mu_s = 0.6$ and 0.75, the optimal reshear criteria in a compressional regime are then, respectively:

$$(\sigma_1 - \sigma_3) = 2.12\sigma'_v \quad \text{and} \quad (\sigma_1 - \sigma_3) = 3\sigma'_v \quad (18)$$

while for an extensional regime, they are:

$$(\sigma_1 - \sigma_3) = 0.68\sigma'_v \quad \text{and} \quad (\sigma_1 - \sigma_3) = 0.75\sigma'_v. \quad (19)$$

CONSTRUCTION OF THE BRITTLE FAILURE PLOTS

On the basis of these equations, the differential stress, $(\sigma_1 - \sigma_3)$, required for different modes of brittle failure can be plotted against effective vertical stress, σ_v', as composite failure curves for various values of tensile strength, T, in compressional ($\sigma_v = \sigma_3$) and extensional ($\sigma_v = \sigma_1$) tectonic regimes (Fig. 2). The failure criteria for extensional fracturing (equations 7 and 8) hold over the range, $0 < (\sigma_1 - \sigma_3) < 4T$; those for the Griffith criterion (equations 10 and 11) over the range, $4\,T < (\sigma_1 - \sigma_3) < 6.66\,T$ (note that this includes both extensional and compressional shear failure); and those for the Coulomb shear failure criterion (equations 13 and 14) over the range, $(\sigma_1 - \sigma_3) > 6.66\,T$. Expected orientations of brittle structures resulting from the three different modes of failure are illustrated for both the compressional and extensional plots.

Differential stress values required for reshear of optimally oriented cohesionless faults in compressional and extensional tectonic regimes (equations 18 and 19) are also shown for comparison. Note how with increasing tensile strength, the composite failure curves move progressively further from the optimal reshear condition. Laboratory determinations of tensile strength generally yield values in the range 1–10 MPa for sedimentary rocks but crystalline rocks may have tensile strengths of 20 MPa or more (Lockner, 1995). Long-term values of tensile strength of rocks, however, may be only a fraction of the laboratory determined values.

In Fig. 2(c), the pore-fluid factor, λ_v, is plotted against effective vertical stress, σ_v', and contoured in depths, z, to define (from equation (3) the possible depth and fluid-pressure combinations corresponding to particular σ_v' values. $\lambda_v = 0$ corresponds to dry crust; $\lambda_v \approx 0.4$ to hydrostatic conditions for a crustal density, $\rho = 2550$ kg/m^3; $0.4 < \lambda_v < 1.0$ to suprahydrostatic conditions; $\lambda_v = 1.0$ to lithostatic fluid pressure levels; and $\lambda_v > 1.0$ to supralithostatic conditions. A horizontal line corresponding to a particular σ_v' value defines the locus of possible z and λ_v combinations. Thus, a σ_v' value of 60 MPa, representing the maximum depth for pure extension fractures when $T = 20$ MPa in an extensional regime, corresponds to depths of 2.4 km in dry crust ($\lambda_v = 0$), 4 km under hydrostatic conditions ($\lambda_v = 0.4$), 6 km when $\lambda_v = 0.6$, or 8 km when $\lambda_v = 0.7$.

DISCUSSION

In considering these 'generic' failure mode plots, it is important to keep in mind the assumptions involved in their construction. First amongst these is the assumption of uniform 'Andersonian' stress fields with $\sigma_v = \sigma_1$ or σ_3 and no stress heterogenities arising from fault stepovers (e.g. Segall and Pollard, 1980) or other forms of structural or material irregularity. Second is the assumption of a linear Coulomb failure envelope for most of the compressional field when, in reality, most experimentally determined envelopes are gently

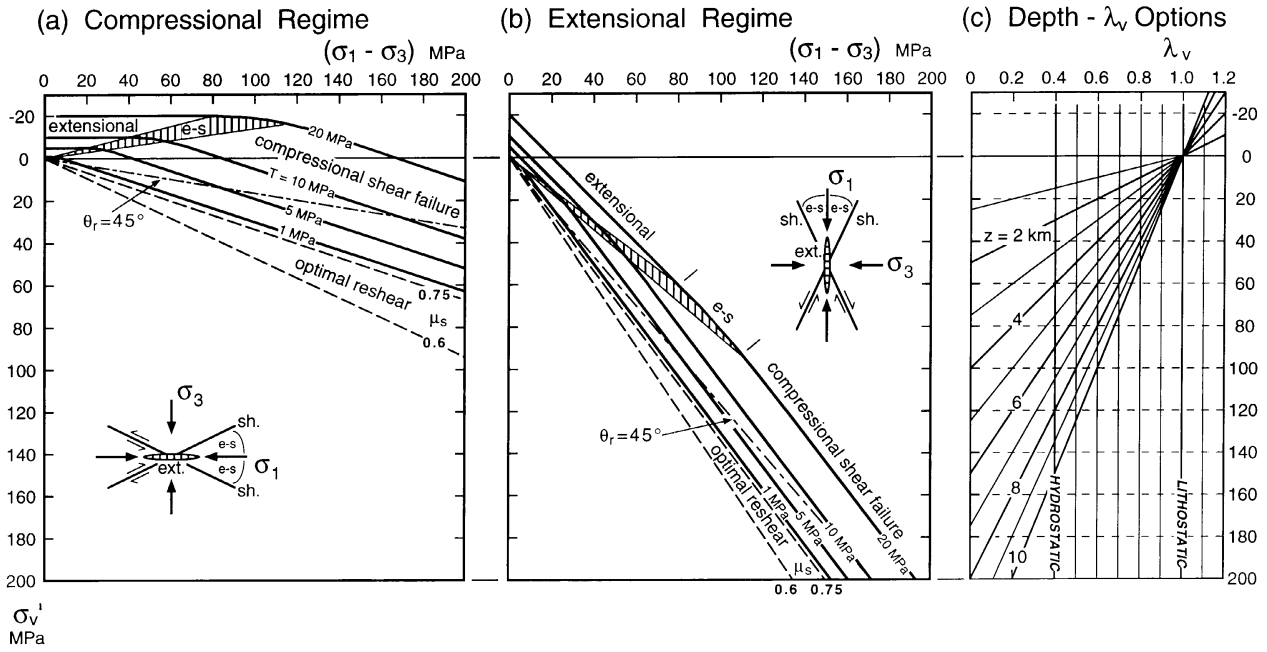

Fig. 2. Brittle failure mode diagrams for: (a) compressional; and (b) extensional tectonic regimes, plotting differential stress at failure, $(\sigma_1-\sigma_3)$, against effective vertical stress, σ_v'. Solid bold lines define the failure conditions for intact rock with various values of tensile rock strength, T. The fields occupied by the different failure modes are labelled on the plots with the fields of extensional-shear failure cross-hatched. Expected orientations of extension fractures (ext.), Coulomb shear fractures or faults (sh.), and extensional shear fractures (e-s) are shown in the insets. Also shown are reshear criteria for optimally oriented cohesionless faults with $\mu_s=0.6$ and 0.75 (dashed lines), and for $\theta_r=45^\circ$ when $\mu_s=0.75$ (dash–dot lines). In (c), values for σ_v' can be equated to specific depth and fluid-pressure combinations.

concave to the σ_n' axis of the Mohr diagram (Jaeger and Cook, 1979). This may lead to an overestimate of the differential stress required for compressional shear failure at depth. Bear in mind also that the tensile strength, T, on the generic failure envelope (Fig. 1), equivalent to roughly half the cohesive strength, represents the long-term tensile strength of the material and may be only a fraction of that determined by comparatively fast strain-rate laboratory tests. Note finally that more complex situations than the simplified 'generic' criteria considered here could be represented by modifying the material parameters and failure equations as necessary.

These considerations notwithstanding, the plots in Fig. 2 represent end-member situations illustrating the marked mechanical contrast between purely extensional and compressional tectonic regimes. Initially intact rock masses are weak under horizontal extension in comparison with compression, with brittle failure occurring at much lower levels of differential stress for the same depth and fluid pressure condition. Under the same λ_v condition, the differential stress required for compressional shear failure at a particular depth in a compressional regime is four times greater than in an extensional regime.

For any value of the pore-fluid factor in an extensional tectonic regime, there is a progression with depth from extensional fracturing through extensional-shear to compressional shear failure. Transition depths between the different failure modes increase with increasing tensile strength. In a compressional regime, by contrast, only compressional shear failure can occur at comparatively high differential stress levels for $\lambda_v<1.0$, and supralithostatic fluid pressures ($\lambda_v>1.0$) are needed to induce all other failure modes. Composite failure mode plots for strike-slip regimes with $\sigma_v=\sigma_2$ may lie anywhere between the compressional and extensional plots, approaching the compressional regime plot as $\sigma_2\rightarrow\sigma_3$, and the extensional plot when $\sigma_2\rightarrow\sigma_1$.

The plots also illustrate how mixed-mode brittle failure may occur under the same differential stress and fluid pressure conditions within a heterogeneous rock mass with varying tensile strength (competence). Under such circumstances, mesh structures comprising interlinked arrays of low displacement faults, extensional-shear fractures, and extension fractures may form under low effective vertical stress (Sibson, 1996). Mixed-mode failure may occur under hydrostatic fluid pressure levels in the near-surface in extensional tectonic regimes, but requires supralithostatic fluid pressures in compressional regimes. It becomes apparent why a 'buried' normal fault commonly 'horsetails' upwards into an array of subvertical extensional and extensional-shear fractures in the near-surface. Gudmunsson (1992), for example, has demonstrated how normal faulting at depth in the Icelandic lava pile leads first to the development of extensional fissures in young surface lavas and then, with progressive slip, to substantial vertical displacements across the gaping subvertical fissures.

Note further how the reshear condition for existing faults that are optimally oriented for frictional reactivation prevents the attainment of the differential stress values needed to induce brittle failure of intact rock. This has the important implication that the different modes of brittle failure in intact rock are only likely to occur in the absence of throughgoing faults that are favourably oriented for reactivation, and may locally predate the development of such structures. Provided that their poles lie within the plane containing σ_1 and σ_3, so that 2-D reactivation theory (equation 16) is applicable, reshear conditions for non-optimally orientated existing faults may also be represented. The reshear condition for a 45° dipping fault ($\theta_r = 45°$) when $\mu_s = 0.75$ is shown on both the compressional and extensional plots in Fig. 2. With increasing σ_v', there is a crossover value for a particular tensile strength above which reshear of the existing fault will occur at lower differential stress than that required for intact rock failure, and below which the reverse is true.

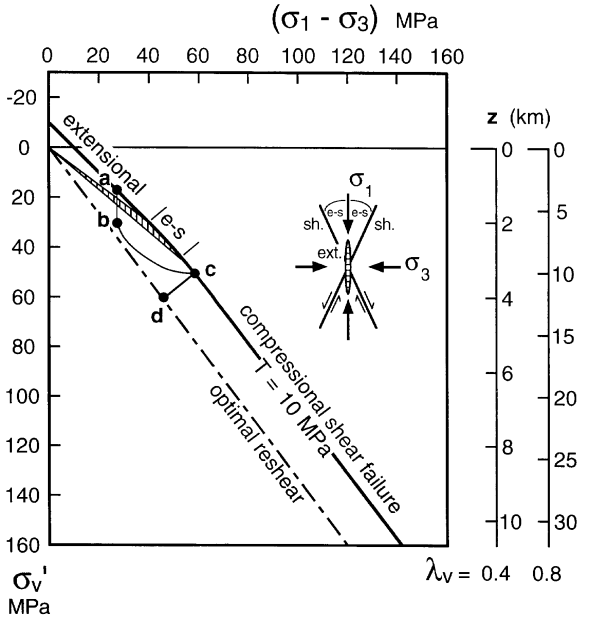

Fig. 3. Extensional failure plot illustrating changing brittle failure modes for a competent bed undergoing progressive extension along the path a–b–c–d in an initially overpressured sedimentary basin (see text).

APPLICATIONS

These plots defining the stress and fluid-pressure fields for different modes of brittle rock failure in compressional and extensional tectonic regimes have wide application. From the viewpoint of basic structural mechanics they emphasize the critical role of fluid pressure in developing or reactivating brittle structures and illustrate how very much easier it is, in terms of both differential stress and fluid pressure level, to induce brittle failure within a rock mass undergoing horizontal extension in comparison with one undergoing horizontal shortening.

Fault and fracture development in sedimentary basins

It is apparent that while extension fracture permeability may develop under hydrostatic fluid pressures in the near-surface of extensional sedimentary basins, development of comparable fracture permeability in compressional settings such as foreland basins requires fluids overpressured to supralithostatic values, unless marked stress heterogeneity exists. Note further how interlayered strata with contrasting tensile strengths may deform through a mixture of different brittle failure modes under comparatively low values of effective vertical stress in extensional settings (and negative values in compressional settings).

The plots may also be used to consider time progressions in failure mode. Arrays of hydraulic extension fractures commonly form in overpressured portions of extensional sedimentary basins undergoing compaction prior to the development of throughgoing normal faults (e.g. Peacock and Sanderson, 1991). Consider a hypothetical deformation path (a–b–c–d) for a competent bed with tensile strength, $T = 10$ MPa, within such a basin that is undergoing progressive extension (Fig. 3). Initial hydrofracturing (a) occurs at a depth of 4 km with $\lambda_v = 0.8$ under comparatively low differential stress, leading to fluid loss through vertical extension fractures, a drop in fluid pressure level, and an increase in σ_v' (b). Increasing differential stress through progressive regional extension, coupled with further fluid loss, then brings about a change to compressional shear failure (c) which leads to a reduction in differential stress. Once optimally oriented cohesionless faults are established (d) with fluid pressure dropping to hydrostatic ($\lambda_v = 0.4$), no further hydraulic fracturing is possible unless the faults heal and regain cohesive strength through hydrothermal cementation, allowing fluid overpressures to reaccumulate at depth.

Basin inversion

During basin inversion, steeply-to-moderately dipping normal faults originally developed through progressive extension are sometimes reactivated as reverse faults during subsequent compression. Reactivation criteria for particular fault dips (e.g. the $\theta_r = 45°$ example in Fig. 2) may be employed to evaluate the particular stress and fluid-pressure conditions under which reactivation of the existing faults will occur in preference to the formation of new favourably oriented structures.

Brittle structures hosting mineralization

The plots also have relevance to mineralization processes, emphasizing the critical role of fluid pressure and tectonic stress at different crustal levels. Much hy-

drothermal mineralization is hosted in fault–fracture meshes comprising arrays of parallel extensional fractures interlinked by faults. Formation of these mesh structures, which act as high permeability conduits for large-volume fluid flow, involves mixed-mode brittle failure with hydraulic extension fractures forming in higher tensile strength rock and faulting in weaker material (Sibson, 1996). The condition for mesh development is therefore approximated by the hydraulic fracture criterion (equation 6) which must be satisfied, at least locally.

Under hydrostatic fluid pressures, in the absence of strong stress heterogeneity, hydraulic extension fracturing can only occur in the near-surface of extensional (or transtensional) tectonic regimes (Fig. 2), the characteristic setting for epizonal mineralization formed from upwelling geothermal plumes that are close to hydrostatically pressured (Henley, 1985). Explorationists have also recognized 'ground preparation' from silica flooding as a precursor to the development of significant deposits in the epizonal environment. This has considerable mechanical significance. Silicification imparts higher tensile strength, allowing a greater depth range for extensional fracturing (Fig. 2) and, through the clogging of pore and fracture space, may also lead to local fluid overpressuring in hydrothermal systems.

At greater depths, formation of comparable high-permeability conduits requires either strong stress heterogeneity or varying degrees of fluid overpressuring, depending on the tectonic regime. The large mesozonal lode gold deposits that characterise Archean granite–greenstone assemblages, and their younger analogues (e.g. Paleozoic mineralization in Victoria, Australia, Cretaceous mineralization in the Mother Lode belt of the Sierra Nevadan foot hills in California, and Eocene mineralization within the Juneau gold belt of S.E. Alaska) typically developed in compressional or transpressional tectonic settings in the depth interval 5–15 km (Groves, 1993; Hodgson, 1993). Many of these vein systems comprise a mesh of veins occupying steep reverse faults and flat-lying hydraulic extension fractures. The fault–fracture meshes hosting these vein systems apparently developed towards the base of the upper brittle crust under near-lithostatic levels of fluid pressure (Sibson *et al.*, 1988; Cox, 1995; Robert *et al.*, 1995).

Note, however, that substantial overpressuring above hydrostatic may occur without leaving any macrostructural record; direct evidence for overpressuring in the form of extension veins formed by hydraulic fracturing only occurs for the extreme cases when $P_f > \sigma_3$. Overpressures significantly above hydrostatic may still greatly enhance permeability and fluid flux (Zhang *et al.*, 1994) and contribute to mineralization without the hydrofracture condition being attained.

Acknowledgements—I thank Chris Scholz and Dave Sanderson for constructive reviews. This research was funded by the NZ Public Good Science Fund through FRST Contract ♯CO5611 during sabbatical leave from the University of Otago. Hospitality extended by Professor Rob Knipe of the Rock Deformation Research Group at the University of Leeds, UK, and by Professors Bruce Luyendyk and Ralph Archuleta of the Department of Geological Sciences at the University of California, Santa Barbara, USA, is gratefully acknowledged.

REFERENCES

Anderson, E. M. (1951) *The Dynamics of Faulting and Dyke Formation with Application to Britain*, 2nd edn. Oliver and Boyd, Edinburgh.

Brace, W. F. (1960) An extension of the Griffith theory of fracture to rocks. *Journal of Geophysical Research* **65,** 3477–3480.

Byerlee, J. D. (1978) Friction of rocks. *Pure and Applied Geophysics* **116,** 615–626.

Cox, S. F. (1995) Faulting processes at high fluid pressures: an example from the Wattle Gully Fault, Victoria, Australia. *Journal of Geophysical Research* **100,** 12841–12859.

Griffith, A. E. (1924) Theory of rupture. In *Proceedings of the First International Congress on Applied Mechanics, Waltman, Delft*, eds C. B. Biezeno and J. M. Burgers, pp. 53–63.

Groves, D. I. (1993) The crustal continuum model for late Archean lode gold deposits of the Yilgarn block, Western Australia. *Mineralium Deposita* **28,** 366–374.

Gudmunsson, A. (1992) Formation and growth of normal faults at the divergent plate boundary in Iceland. *Terra Nova* **4,** 464–471.

Hancock, P. L. (1985) Brittle microtectonics: principles and practice. *Journal of Structural Geology* **7,** 437–457.

Henley, R. W. (1985) The geothermal framework of epithermal deposits. In *Geology and Geochemistry of Epthermal Systems*, ed. B. R. Berger and P. M. Bethke. Society of Economic Geologists Reviews in Economic Geology **2,** pp. 1–24.

Hodgson, C. I. (1993) Mesothermal lode gold deposits. *Geological Association of Canada Special Paper* **40,** 635–678.

Hubbert, M. K. and Rubey, W. W. (1959) Role of fluid pressure in mechanics of overthrust faulting. *Bulletin of the Geological Society of America* **70,** 115–166.

Jaeger, J. C. and Cook, N. G. W. (1979) *Fundamentals of Rock Mechanics*, (3rd edn) edn. Chapman & Hall, London.

Lockner, D. A. (1995) Rock Failure. In *Rock Physics and Phase Relations: A Handbook of Physical Constants*. AGU Reference Shelf **3,** pp. 127–147.

Lockner, D. A. and Byerlee, J. (1993) How geometrical constraints contribute to the weakness of mature faults. *Nature* **363,** 250–252.

Peacock, D. C. P. and Sanderson, D. J. (1991) Displacements, segment linkage and relay ramps in normal fault zones. *Journal of Structural Geology* **13,** 721–733.

Robert, F., Boullier, A-M. and Firdaous, K. (1995) Gold–quartz veins in metamorphic terranes and their bearing on the role of fluids in faulting. *Journal of Geophysical Research* **100,** 12,861–12,879.

Secor, D. T. (1965) Role of fluid pressure in jointing. *American Journal of Science* **263,** 633–646.

Segall, P. and Pollard, D. D. (1980) Mechanics of discontinuous faults. *Journal of Geophysical Research* **85,** 4337–4350.

Sibson, R. H. (1985) A note on fault reactivation. *Journal of Structural Geology* **7,** 751–754.

Sibson, R. H. (1996) Structural permeability of fluid-driven fault-fracture meshes. *Journal of Structural Geology* **18,** 1031–1042.

Sibson, R. H., Robert, F. and Poulsen, K. H. (1988) High-angle reverse faults, fluid-pressure cycling, and mesothermal gold–quartz deposits. *Geology* **16,** 551–555.

Zhang, S., Cox, S. F. and Paterson, M. S. (1994) The influence of room temperature deformation on porosity and permeability in calcite aggregates. *Journal of Geophysical Research* **89,** 15761–15775.